Hindawi
Advances in Materials Science and Engineering
Volume 2018, Article ID 3954163, 9 pages
https://doi.org/10.1155/2018/3954163

Research Article

Shape Stability of Polyethylene Glycol/Acetylene Black Phase Change Composites for Latent Heat Storage

Jingjing Zhang[1], **Hairong Li**[2], **Junyang Tu**[1], **Ruonan Shi**[1], **Zhiping Luo**[1,3], **Chuanxi Xiong**[1], **and Ming Jiang**[1]

[1]*School of Materials Science and Engineering, State Key Lab for New Textile Materials and Advanced Processing Technology, Wuhan Textile University, Wuhan 430200, China*
[2]*Mechanical Metrology Division, Hubei Institute of Measurement and Testing Technology, Wuhan 430223, China*
[3]*Department of Chemistry and Physics, Fayetteville State University, Fayetteville, NC 28301, USA*

Correspondence should be addressed to Hairong Li; ronghailee@163.com and Ming Jiang; mjiang@wtu.edu.cn

Received 1 August 2018; Accepted 1 October 2018; Published 24 October 2018

Academic Editor: Veronica Calado

Sufficient shape stability is essential for a high-performance phase change material (PCM). Although significant advances have been made to develop form-stable composites, technical development in the field of polymer-based PCMs is currently limited by an incomplete understanding of the shape stability. Form-stable polyethylene glycol/acetylene black (PEG/AB) PCMs containing PEGs with different average molecular weights have been obtained by melt mixing to investigate the shape stability of the PEG/AB composites. It was found that the phase change behaviors of the PEG/AB composites were not only attributed to the interactions between the AB and PEG, but also to the intermolecular interactions of the PEG chains, depending on the varying molecular weights of the PEGs. Physically crosslinked structure with temporary junctions was formed through hydrogen bonding, capillary, surface tension forces, intermolecular friction, and macromolecular entanglement, which contributed to the constrained chain motion and thus the solid-solid phase change behavior of the PEG/AB composites. The physically crosslinked structure was more stable with longer length of the PEG molecular chains, resulting in higher critical impregnated contents of the PEG into the AB and thus improved latent heat.

1. Introduction

Energy storage can optimize the energy flows to overcome the mismatch between the demand for energy and the supply of energy, especially for energy generated by variable and renewable resources, such as water, wind, and solar energy [1]. Among the principal energy-storage technologies, phase change materials (PCMs) have drawn tremendous attention because they can store and release large amounts of latent heat as they change from one physical state to another for effective use of thermal energy [2–5]. To increase the energy-storage ability, PCMs with large latent heat are essential for future thermal energy storage and management [6, 7].

Among the PCMs investigated, polyethylene glycol (PEG) is one of the prospective candidates in this regard as it exhibits relatively high latent heat-storage capacity, tunable solid-liquid phase change temperature, and non-corrosiveness, which leads to compact storage devices with high energy-storage density. Moreover, PEG has much better cycling stability during services and higher security than small-molecule organic PCMs due to nondetectable vapor pressure when melts [8–11]. Nevertheless, as a solid-liquid PCM, the applications of PEG are largely limited, as the liquid phase leaks above the phase change point. The leakage is usually circumvented by introducing form-stable support. Considerable efforts have been devoted to develop form-stable composites with high energy-storage densities [12–23]. The form stabilization strategies of PCMs include encapsulation [12, 13], grafting [14, 15], and physical adsorptions [16–23]. Clay, diatomite, halloysite, active carbon, silica, expanded graphite, and graphene have been employed as fillers to prevent melted PCMs from leaking during the

phase transition via physical adsorptions, relying on their predominantly polar surface and/or high porous structures [16–23]. However, although significant advances have been made, technical development in the field of polymer-based PCMs is currently limited by an incomplete understanding of the shape stability. The affinity of support fillers to PCMs depends on their structures, so the structure of the fillers usually is a primary consideration for the shape stability. Thus far, few attentions have been paid on the difference in shape stabilities between polymeric PCMs and low molecular weight organic PCMs. The effect of some critical structure factors for polymeric PCMs, such as molecular weight, on the shape stability was largely neglected. However, the shape stability of polymer-based composite PCMs could not be entirely determined by the affinity of support fillers to PCMs or the interactions between them and might be partly attributed to the structure of the polymeric PCMs. Therefore, a further understanding of the form stabilization mechanisms would ultimately produce a more rational and general approach to the thermal property optimisation of PEG-based composite PCMs.

The present work is an attempt to develop a better understanding of the shape stability of polymeric PCM-based composites by comparing the effects of PEGs with different molecular weights (M_w) on the thermal properties of PCM composites filled by commercially available acetylene black (AB). The phase change behaviors of the form-stable PEG/AB PCMs were verified by polarized optical microscopy (POM) and filter paper test. Furthermore, the structures and thermophysical properties of the composite PCMs were analyzed by scanning electron microscopy (SEM), X-ray diffractometer (XRD), thermogravimetric analysis (TGA), and differential scanning calorimetry (DSC). Finally, the existence of an intermolecular interaction mechanism of solid-solid phase change besides simple physical adsorptions in the PEG/AB composite PCMs was found.

2. Materials and Methods

2.1. Materials. Chemically pure PEGs were purchased from Sinopharm Chemical Reagent Beijing Co., Ltd. PEG800, PEG4000, PEG6000, and PEG10000 were utilized in this work. AB (purity > 99.99%, particle size = 150–200 nm based on the supplier's information) was purchased from Shanghai Chemical Reagent Co. Ltd. and used after drying.

2.2. Preparation of PEG/AB Composites. To fabricate the PEG/AB composites, the PEGs with various average molecular weights were first melt at 50–70°C, and then the AB was slowly added under stirring and vacuum. Finally, the mixture was dried in a vacuum oven at 70°C for 48 h.

2.3. Characterization. The Fourier-transform infrared (FTIR) spectrum was observed at room temperature (Thermo Nicolet Nexus) in the range of 4,000 to 400 cm^{-1} using KBr pellets. Nitrogen adsorption/desorption isotherms were measured on a Micromeritics Model TriStar II 3020 volumetric analyzer (USA). POM observation was conducted on an Olympus BX51-P polarizing optical microscope equipped with a LTS 350 hot stage. TGA was carried out on a TG/DTA 220U (Seiko Instrument Co. Ltd, Tokyo Japan) with the Exstar 6000 Station. The samples were scanned from 20 to 800°C with the heating rate of 10°C/min and nitrogen gas purging. The X-ray measurements were carried out on a Rigaku D/Max-IIIA X-ray diffractometer with Cu-Kα radiation at a wavelength of 1.54 Å. Thermal analysis was performed using a DSC (PE Co., USA). The thermal conductivities of the various samples were measured at 28°C by the guarded heat flow test method (TA Instruments DTC 300, USA). Thermograms were obtained at a heating and cooling rate of 5°C·min^{-1} at a temperature range from 20°C to 80°C under nitrogen atmosphere. To confirm the reproducibility of the results, at least two samples were measured for each composition. For each sample, at least three DSC traces were recorded. SEM measurements were performed with JSM-IT300A (JEOL Ltd., Japan).

3. Results and Discussion

3.1. Chemical and Physical Characterizations of the AB Particles. Chemical characterizations of the AB particles and the PEG/AB composites are carried out using FTIR spectroscopy, as shown in Figure 1. In the spectrum of the AB (Figure 1(a)), the peaks at 2,888 cm^{-1}, 1,146 cm^{-1}, and 1,114 cm^{-1} represent the stretching vibration of C-O groups. The peak at 1,637 cm^{-1} is attributed to C=O stretching vibration. O-H stretching vibrations are characterized by the broadband in the region of 3,300–3,650 cm^{-1}. The spectrum of pristine PEG (Figure 1(b)) is characterized by O-H stretching vibration at 3433 cm^{-1} and the strong absorption peaks of C-H bonds at 2888 cm^{-1}, 953 cm^{-1}, and 839 cm^{-1}. The C-O stretching vibration was at 1106 cm^{-1}. The FTIR results indicate that no significant new peaks were observed other than characteristic peaks of PEGs and AB at FTIR spectrums of the PEG/AB composites (Figure 1(b)), which proves that the interactions between the functional groups of PEG and AB are physical in nature. Moreover, the existence of weak hydrogen bonding between the AB and PEG, which could be able to increase PEG-absorbing capacity of the AB to some extent.

To further examine the pore adsorption capacity of the AB particles, nitrogen adsorption/desorption isotherms are measured. The pore-size distribution of the AB is shown in Figure 2. The AB particles possess a specific Brunauer–Emmett–Teller (BET) surface area of 53.79 m^2/g, with a most probable pore size of about 2.6 nm. The specific surface area is much lower than those of porous carbon materials, such as expanded graphite or active carbon. Moreover, the average pore size of the AB particles is smaller than the equivalent sphere diameter of PEG4000 or PEG with higher M_w. The equivalent radius of PEG random coils can be calculated according to previous reports [24]. The above analysis shows a relatively low pore adsorption capacity of the AB particles.

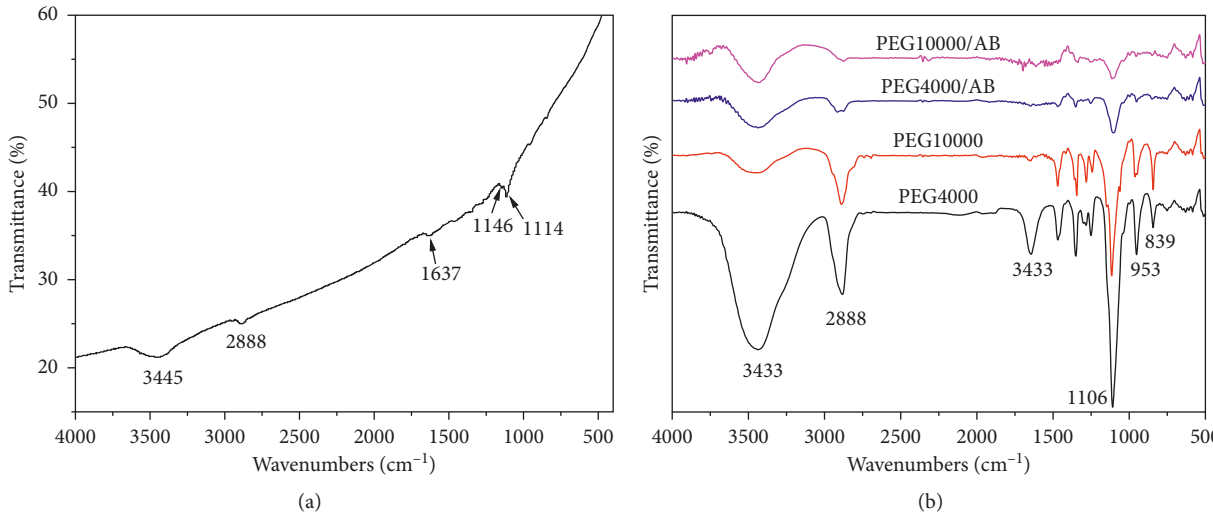

Figure 1: FTIR spectrums of the AB particles (a) and PEG/AB composites (b).

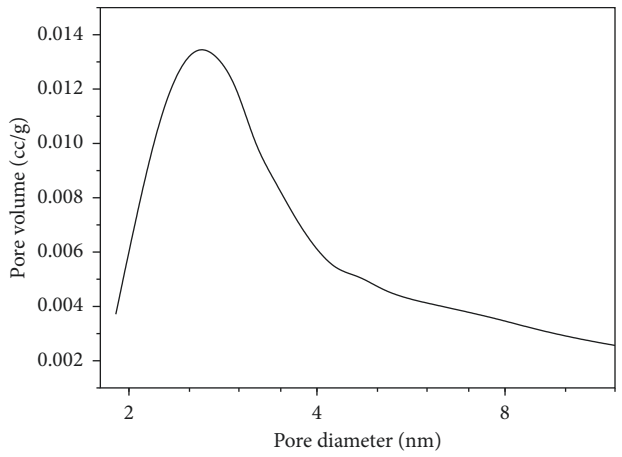

Figure 2: Pore-size distribution of the AB particles.

3.2. Leakage Behavior of the PEG/AB Composites. The leakage behavior of the PEG/AB composites is investigated by POM and filter paper test. The POM images are taken below the crystallization temperature of the PEG10,000/AB composites, as shown in Figure 3. The darker regions correspond to the saturated AB, whereas the lighter regions marked by arrows indicate the excess PEG, as shown in Figure 3(a). When the mass fraction of the AB is increased to 11.6 wt.%, the excess PEG1,000 cannot be observed in the POM image in Figure 3(b), indicating the complete absorption of the PEG in the AB particles.

The leakage behavior of the PEG/AB composites at elevated temperature above the phase change point is further studied. Typically, the PEG/AB samples are kept in filter paper envelopes above the phase change temperatures for 1.5 h and the change in the weight of the filter paper envelopes before and after the test are measured, and the results were presented in Table 1. No significant change in weight is observed under 80°C, indicating that no obvious PEG leakage occurred during the test. Consequently, the optimum absorption ratio of PEG800, PEG4,000, PEG6,000, and PEG10,000 in AB should be around 0.76, 0.84, 0.87, and 0.88 (responding to the results obtained by TGA below), respectively, and these mass fractions are adequate to obtain form-stable PEG/AB composite PCMs.

3.3. Thermal Reliability of the PEG/AB Composites. The TG curves of the pure PEG and PEG/AB composite PCMs are shown in Figure 4. As can be seen from the curves, all samples have a single thermal degradation stage. The degradation of the PEGs with relatively large molecular weights and their composite PCMs starts around 350°C and ends at 430°C, while the PEG800 starts below 300°C and ends at 430°C. It indicates that the AB does not significantly affect the thermal stability of the PEGs with relatively large M_w but improves the thermal stability of PEG with relatively small M_w (PEG800). This is attributed to the stronger interaction between AB and PEG800 induced by pore adsorption due to the smaller equivalent sphere diameter of PEG800 than the average pore size of AB. That is, the PEG chains are trapped inside the AB pores. In addition, these results also demonstrate that no chemical reactions take place during simple melt blending and impregnation process. Moreover, the TG curves of the form-stable composite PCMs also confirm the optimum impregnation ratios of PEG800, PEG4,000, PEG6,000, and PEG10,000 as 76.4 wt%, 83.9 wt%, 86.8 wt%, and 88.4 wt%, respectively.

3.4. Crystalline Properties of the PEG/AB Composites. The XRD patterns of the PEG and PEG/AB composites at room temperature are displayed in Figure 5. It is observed that the AB only has a weak and broad peak at 25°, indicating an amorphous structure. The XRD patterns of the PEG4,000, PEG6,000, and PEG10,000 are characterized by two strong 2θ peaks at 19.1° and 23.6°, which are assigned to the typical plane of (120) and (112) of the PEGs. The XRD curves of the PEG/AB composites are similar to those pure PEGs, and the position of the diffraction peaks remains unchanged after the

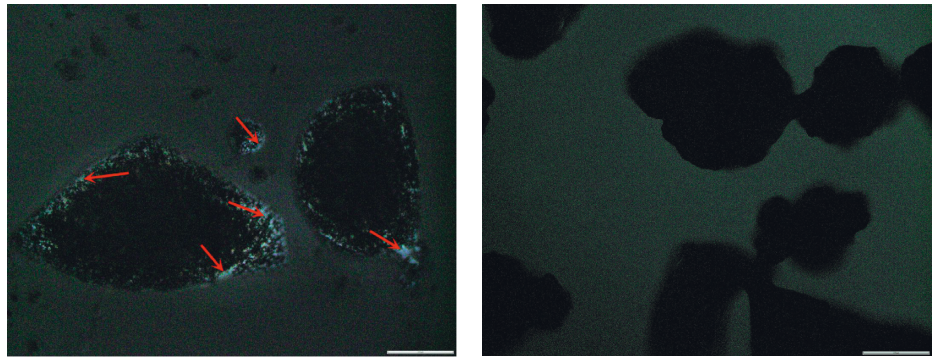

(a) (b)

Figure 3: POM images taken below the crystallization temperature of PEG10000/9 wt.%AB (a) and PEG10000/11.6 wt.%AB (b) Scale bar: 100 μm.

Table 1: Relative weight changes of the PEG/AB composites before and after the leakage tests at 80°C for 1.5 h.

Samples	Average weight $_{before}$ (mg)	Average weight $_{after}$ (mg)	Δ (%)	Standard deviation (mg)
PEG800/AB	313.2	317.2	1.27	0.88
PEG4000/AB	318.5	321.2	0.85	0.31
PEG6000/AB	319.4	322.7	1.03	0.76
PEG10000/AB	312.3	315.3	0.96	0.56

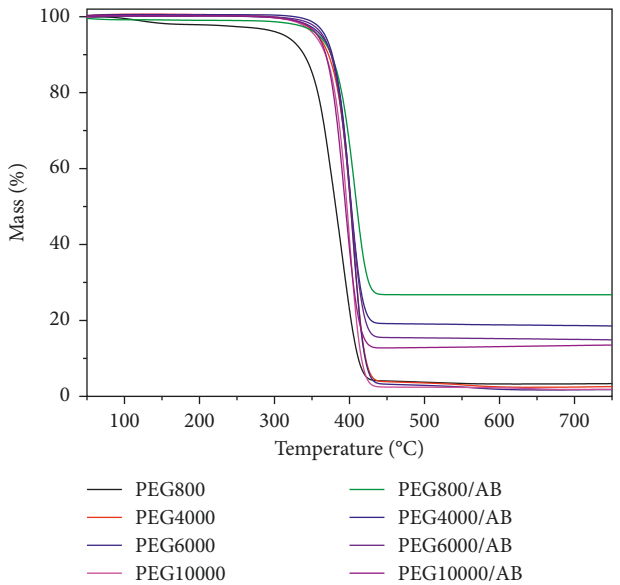

Figure 4: TG plots of the PEGs and PEG/AB composites.

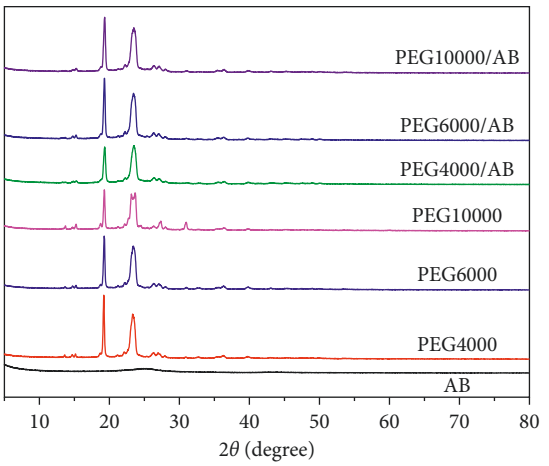

Figure 5: XRD spectra of the AB, pristine PEGs, and PEG/AB composites.

melt blending process, which demonstrates that the pristine PEG and the PEG/AB have the similar crystal structure and crystal cell type.

3.5. Thermal Conductivities of the PEG/AB Composites. The thermal conductivities of different mass ratios of AB are presented in Figure 6. It can be seen that almost linear correlation exists between the thermal conductivity and content of the AB for each PEG system. A slow increase in thermal conductivity from ~0.15 W/mK to ~0.26 W/mK with the increase of the mass ratio of the AB is observed due to the intrinsically low thermal conductivity of the AB induced by its amorphous structure. AB is chosen as the supporting material to verify the effect of molecular weight of PEG on the shape stability so as to exclude the strong interactions between PEGs and supporting material, but actually it is not a promising thermally conductive filler for PCMs.

3.6. Thermal Performances of the PEG/AB Composites. The latent heat and phase change temperature of the samples are measured using DSC. Figure 7 shows the melting and freezing DSC curves of the pristine PEGs and form-stable PEG/AB

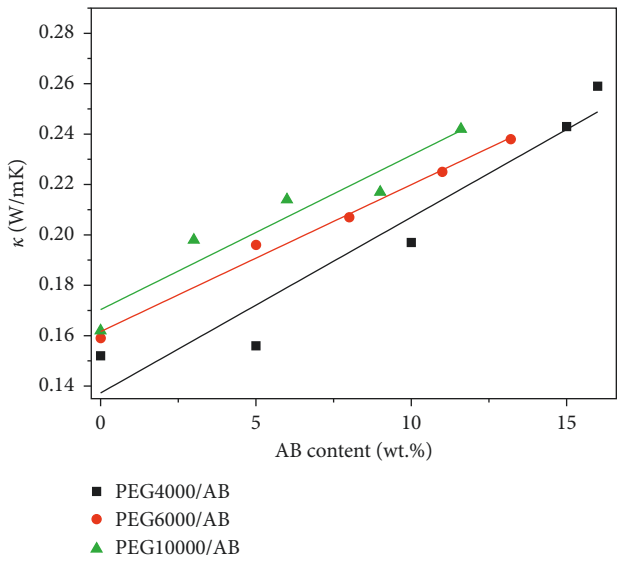

Figure 6: Thermal conductivities with various mass ratios of AB.

composite PCMs. The detailed results of DSC thermal analysis of the peak melting/crystallization temperature (T_m/T_c) ratio, the measured melting/crystallization enthalpy ($\Delta H_m/\Delta H_c$), and the theoretical melting/crystallization enthalpy ($\Delta H_m{}^*/\Delta H_c{}^*$) obtained are presented in Table 1. The theoretical melting/crystallization enthalpies of the PEG/AB composites are calculated based on the impregnated contents of the PEG into the AB and the measured melting/crystallization enthalpies of pristine PEGs, assuming that the AB cannot contribute to the phase change latent heat.

The latent heat capacities of the composite PCMs containing the PEGs with different M_w are obviously lower than those of the pristine PEGs due to the incorporation of the AB that does not undergo phase change. Consequently, in most cases in this study, the melting enthalpies of the PEG/AB composites almost show agreement with the relevant mixture rules. The measured latent heats of the PEG/AB composites with varying PEG M_w from ~4,000 to ~10,000 are comparable with the theoretical latent heats. By adding a proper loading of the AB, relatively high latent heats are retained, especially for the PEG/AB composites containing the PEGs with relatively large M_w. The incorporation of the AB does not induce a significant change of the crystal structure of the PEG with relatively large M_w. Notably, in the case of the PEG800/AB composite, the melting enthalpy is significantly lower by 55.7% than the theoretical value at the optimum loading ratio. This is partially expected given that some of the PCM weight (23.6%) is replaced by the AB particles that are not subject to phase change. In addition, it is quite possible that other mechanisms also affect the phase change process of the PEG800 in the PEG800/AB composites. The presumed reason may be that some of the PEG chains are trapped inside the AB pores when M_w of the PEG is low (PEG800) due to the small equivalent sphere diameter of PEG800 compared to the most probable pore size of the AB. The phase transition of the PEG from amorphous phase into stable crystal phase can be inhibited to a large extent due to the confined chain motion of the PEG induced by the strong adsorbability of the AB pores, and thus the obviously reduced latent heat of phase change is detected by DSC. As a result, the phase change of the composite is prone to take place at lower temperature (Table 2). After AB incorporation, the changes in crystallization temperature identify their tendency to supercool when cooling. However, the incorporation of the AB does not induce a significant supercooling of the PEGs with relatively large M_w because of decreased restriction from the AB pores. By contrast, when the M_w of the PEG increased to ~4,000, most of the PEG chains are completely outside of the AB pores. These chains, different from both the free PEG chains and the chains trapped into the AB pores, are confined by the surface of the AB particles. The longer PEG chains may offer more interacting site for the surface absorption of the PEG on the AB particles. Furthermore, it should be noted that the optimum impregnation ratios of the PEG into the AB for the PEG/AB composites increase with higher M_w of the PEG. These imply the existence of some other mechanisms leading to solid-solid phase change in the PEG/AB composite PCMs besides physical adsorptions. The phase change behavior of the PEG as a polymeric PCM is significantly different from small-molecule PCM, namely, much stronger intermolecular interactions than them. It thus explains in terms of the stronger intermolecular interactions, such as intermolecular friction and macromolecular entanglement, between the PEG4000 chains than those of the PEG800. Therefore, both the critical impregnated content of the PEG into the AB and enthalpy of the PEG4000/AB composite increase remarkably. When M_w increases to ~6,000, the confinement effect from intermolecular interactions is strengthened further with the increase of chain length, and thereby the declining amplitude in T_m of the PEG/AB composite is reduced; the critical impregnated content of the PEG into the AB also shows an increasing trend. With the increase of M_w to 10,000, the critical impregnated content of the PEG into the AB increases further and thus the enthalpy of the PEG10,000/AB composite is improved as well. In other words, the phase change behaviors for the PEG/AB composites are not only attributed to the interactions between the AB and PEG, but also to the intermolecular interactions of the PEG chains depending on the varying M_w of the PEG. The optimum absorption ratio of the PEG in the form-stable PEG800/AB, PEG4,000/AB, PEG6,000/AB, and PEG10,000/AB composite PCMs reaches 0.76, 0.84, 0.87, and 0.88, respectively.

3.7. Shape-Stability Model of the PEG/AB Composites. A model is proposed to explain the shape stability of the PEG/AB composites, based on a physically crosslinked structure with temporary junctions (Figure 8). A part of PEG

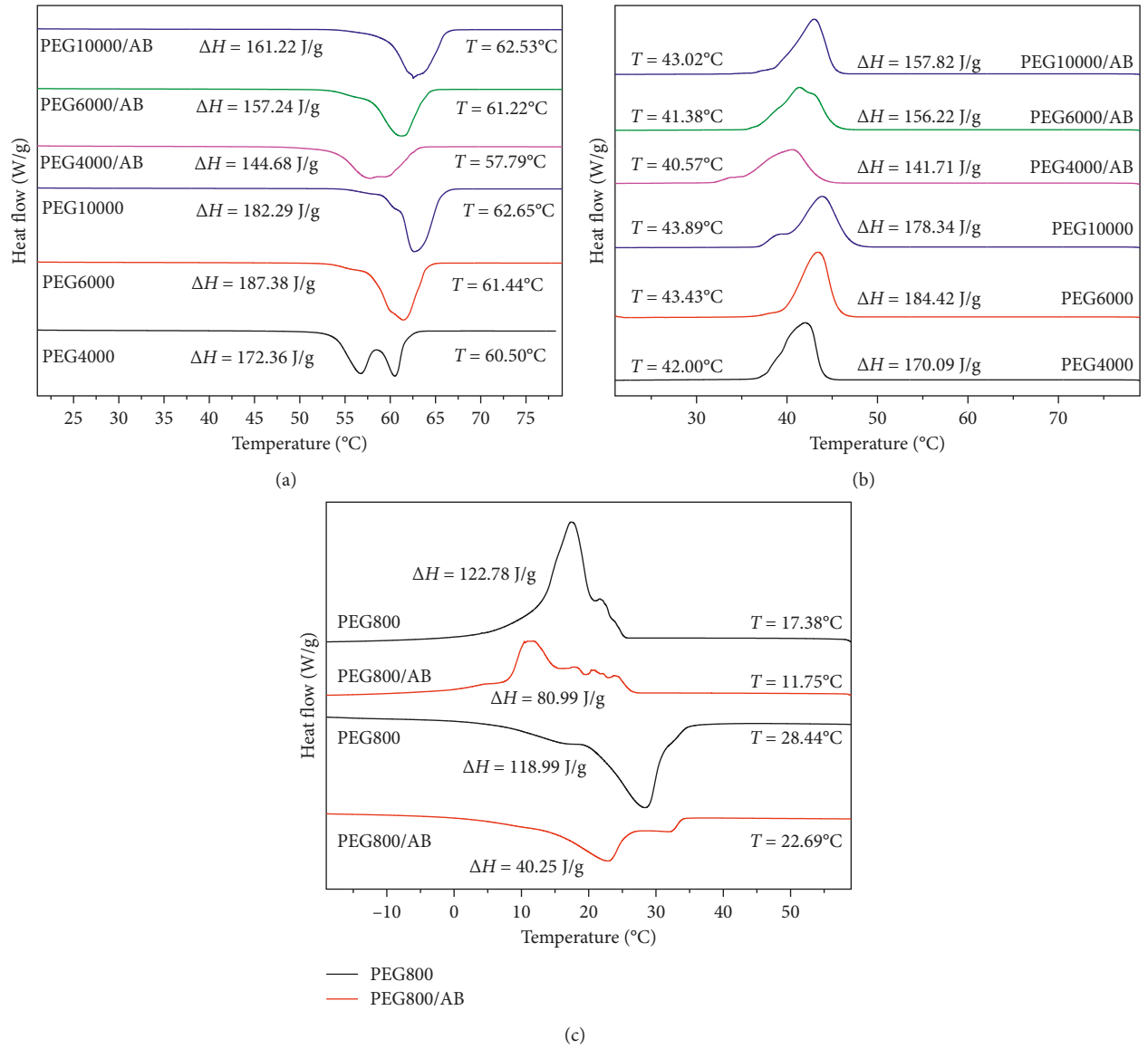

Figure 7: Cyclic DSC heating (a) and cooling (b) curves of pristine PEG4000, PEG6000, PEG10000, and their shape-stabilized PEG/AB composites. (c) DSC curves of PEG800 and PEG800/AB composites.

Table 2: Thermal analysis of the PEG/AB composites and pure PEGs with varying molecular weights.

Samples	Impregnation ratio (wt.%)	T_m (°C)	ΔH_m (J g^{-1})	$\Delta H_m{}^*$ (J·g^{-1})	T_c (°C)	ΔH_c (J·g^{-1})	$\Delta H_c{}^*$ (J·g^{-1})
PEG800	—	28.44	118.99	—	17.38	122.78	—
PEG4000	—	60.50	172.36	—	42.00	170.09	—
PEG6000	—	61.44	187.38	—	43.43	184.42	—
PEG10000	—	62.65	182.29	—	43.89	178.34	—
PEG800/AB	76.40	22.69	40.25	90.91	11.75	80.99	93.80
PEG4000/AB	83.90	57.79	144.68	144.68	40.57	141.71	142.71
PEG6000/AB	86.80	61.22	157.24	162.65	41.38	156.22	160.08
PEG10000/AB	88.40	62.53	161.22	161.14	43.02	157.82	157.65

random coils with small equivalent radius and segments are trapped into the pores of the AB particles by physical interactions, such as capillary and surface tension forces (abbreviated as trapped PEG in Figure 8). In addition, some of the PEG chains that are closely adjacent to the AB are adsorbed on the surface of the AB particles by hydrogen

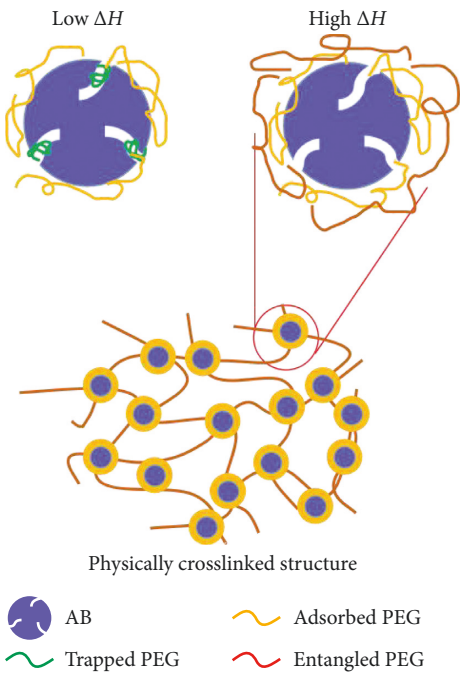

Figure 8: Schematic representation of shape stability.

bonding (abbreviated as adsorbed PEG in Figure 8); and some of the PEG chains with relatively large M_w are stabilized by the macromolecular entanglement and intermolecular friction (abbreviated as entangled PEG in Figure 8). The melting process of the PEG in the composite is confined by a physically crosslinked structure with temporary junctions above T_m of the PEG, which inhibits the phase change of form-stabilized solid phase into liquid phase. The structure becomes more stable with longer length of the PEG molecular chains, resulting in higher critical impregnated content of the PEG into the AB. When the PEG content is increased further above the critical impregnated content, some of the PEG chains would be unbound above the phase change point of the composite, eliminating the shape-stabilized composites.

3.8. Structural Analysis of the PEG/AB Composites. Comparison between the AB and the PEG/AB composites is made by SEM. Figure 9 shows the SEM images of the AB before PCM impregnation and the form-stable PEG/AB composites containing the critical impregnated contents of the PEGs. The morphology of the PEG800/AB composite is similar to that of the AB particles. The AB particles as the supporting material are covered with PEG layers, and the structure of AB framework can be seen because the PEG layer is thin. A part of the PEG800 diffuses into the pores of the AB particles, which is consistent with the DSC results. As discussed before, the PEG molecules with relatively small M_w can be easily trapped by AB, despite the fact that the AB can only provide limited adsorption capability due to the relatively low specific surface area and small pore size. In the case of the composite containing the PEG with relatively large M_w, they appear to follow the different trend. Through SEM analysis, we confirm that most of the PEGs are not dispersed into the pores of the AB. With an increase of M_w to ~4,000 (Figure 9(c)), the AB framework is not obvious since the PEG layer outside of the AB is thicker. When M_w increases to ~6,000 (Figure 9(d)) or ~10,000 (Figure 9(e)), the AB is covered with PEG completely and an irregular morphology can be found since the PEG layer is much thicker due to the longer molecular chain and higher mass fraction of the PEG. Based on the physically crosslinked structure model as discussed above, a part of the PEG segments and random coils with small equivalent radius are trapped into pores of the AB particles by capillary or surface tension forces. The hydrophilic character of the AB particles and cavities in them help us to improve the interfacial compatibility and wetting between the PEG and AB particles; thus some of the PEG chains adjacent to the AB are adsorbed on AB particle surfaces by hydrogen bonding, capillary, or surface tension forces. Other PEG chains are anchored by intermolecular friction and entanglement because there are more chances of intermolecular interactions between the longer PEG chains compared to the PEG with relatively low M_w. Physically crosslinked structure comprising the PEG chains and AB particles is formed through hydrogen bonding, capillary, surface tension forces, intermolecular friction, and macromolecular entanglement, which contributes to constrained chain motion and thus the solid-solid phase change behavior of the PEG/AB composites. Therefore, the optimum impregnation ratio of the PEG into the AB for the PEG/AB composites without seepage of the melted PEG increases with the increasing M_w of the PEG.

4. Conclusions

The PEG/AB composite PCMs exhibited desirable properties in term of shape stability and large latent heats. The AB particles kept the composite form stable without inducing a large reduction in their phase change enthalpies. The fusion enthalpies of the form-stable PEG4,000/AB, PEG6,000/AB, and PEG10,000/AB composite PCMs reached 144.68, 157.24, and 161.22 J/g, respectively. Our results suggest that the phase change behaviors for the PEG/AB composites are attributed not only to the interactions between the AB and PEGs but also to the intermolecular interactions of the PEG chains depending on the varying M_w of the PEGs. The shape stability of the PEG/AB composites were explained based on a physically crosslinked structure model. Physically crosslinked structure with temporary junctions was formed through hydrogen bonding, capillary, surface tension forces, intermolecular friction, and macromolecular entanglement. The structure became stabler with increasing length of the PEG molecular chains, resulting in the increase of the critical impregnated content of the PEG into the AB.

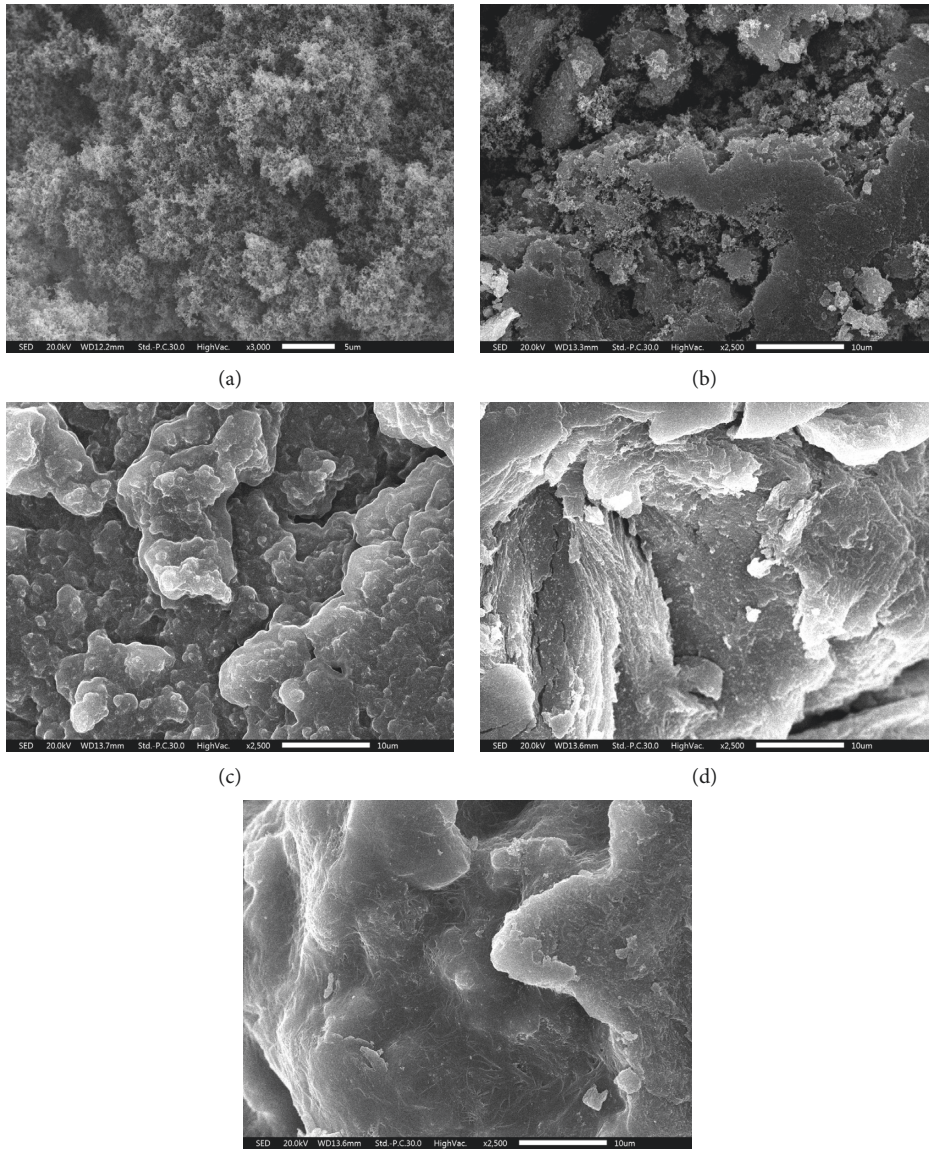

Figure 9: SEM images of the shape-stabilized composite PCMs. (a) AB. (b) PEG800/AB. (c) PEG4000/AB. (d) PEG6000/AB. (e) PEG10000/AB.

Data Availability

The data used to support the findings of this study are available from the corresponding author upon request.

Conflicts of Interest

The authors declare that there are no conflicts of interest regarding the publication of this paper.

Acknowledgments

We gratefully acknowledge the support by the National Natural Science Foundation of China (No. 51503158).

References

[1] Q. Li, L. Chen, M. R. Gadinski et al., "Flexible high-temperature dielectric materials from polymer nanocomposites," *Nature*, vol. 523, no. 7562, pp. 576–579, 2015.

[2] B. Zalba, J. M. Marín, L. F. Cabeza, and H. Mehling, "Review on thermal energy storage with phase change: materials, heat transfer analysis and applications," *Applied Thermal Engineering*, vol. 23, no. 3, pp. 251–283, 2003.

[3] M. Mehrali, S. T. Latibari, M. Mehrali, H. Metselaar, and M. Silakhori, "Shape-stabilized phase change materials with high thermal conductivity based on paraffin/graphene oxide composite," *Energy Conversion and Management*, vol. 67, pp. 275–282, 2013.

[4] A. Abhat, "Low temperature latent heat thermal energy storage: heat storage materials," *Solar Energy*, vol. 30, no. 4, pp. 313–332, 1983.

[5] S. D. Sharma and K. Sagara, "Latent heat storage materials and systems: a review," *International Journal of Green Energy*, vol. 2, no. 1, pp. 1–56, 2005.

[6] Y. Tian and C. Y. Zhao, "A Review of solar collectors and thermal energy storage in solar thermal applications," *Applied Energy*, vol. 104, pp. 538–553, 2013.

[7] A. Váz Sá, R. Almeida, H. Sousa, and J. Delgado, "Numerical analysis of the energy improvement of plastering mortars with phase change materials," *Advances in Materials Science and Engineering*, vol. 2014, Article ID 245473, 13 pages, 2014.

[8] C. Alkan, A. Sari, and O. Uzun, "Poly (ethylene glycol)/acrylic polymer blends for latent heat thermal energy storage," *AIChE Journal*, vol. 52, no. 9, pp. 3310–3314, 2006.

[9] K. Pielichowski and K. Flejtuch, "Differential scanning calorimetric studies on poly(ethylene glycol) with different molecular weights for thermal energy storage materials," *Polymers for Advanced Technologies*, vol. 13, no. 10-12, pp. 690–696, 2002.

[10] S. Han, C. Kim, and D. Kwon, "Thermal degradation of poly (ethylene glycol)," *Polymer Degradation and Stability*, vol. 47, no. 2, pp. 203–208, 1995.

[11] H. Li, M. Jiang, Q. Li et al., "Aqueous preparation of polyethylene glycol/sulfonated graphene phase change composite with enhanced thermal performance," *Energy Conversion and Management*, vol. 75, pp. 482–487, 2013.

[12] X. Jiao, D. Zhao, Y. Zhang et al., "Microencapsulated dimethyl terephthalate phase change material for heat transfer fluid performance enhancement," *Colloid and Polymer Science*, vol. 294, no. 4, pp. 639–646, 2016.

[13] H. Li, M. Jiang, Q. Li et al., "Facile preparation and thermal performances of hexadecanol/crosslinked polystyrene core/shell nanocapsules as phase change material," *Polymer Composites*, vol. 35, no. 11, pp. 2154–2158, 2014.

[14] A. Sarı, C. Alkan, and A. Biçer, "Synthesis and thermal properties of polystyrene-graft-PEG copolymers as new kinds of solid-solid phase change materials for thermal energy storage," *Materials Chemistry and Physics*, vol. 133, no. 1, pp. 87–94, 2012.

[15] R. Cao, H. Liu, S. Chen, D. Pei, J. Miao, and X. Zhang, "Fabrication and properties of graphene oxide-grafted-poly (hexadecyl acrylate) as a solid-solid phase change material," *Composites Science and Technology*, vol. 149, pp. 262–268, 2017.

[16] N. Sarier, E. Onder, S. Ozay, and Y. Ozkilic, "Preparation of phase change material-montmorillonite composites suitable for thermal energy storage," *Thermochimica Acta*, vol. 524, no. 1-2, pp. 39–46, 2011.

[17] X. Fu, Z. Liu, B. Wu, J. Wang, and J. Lei, "Preparation and thermal properties of stearic acid/diatomite composites as form-stable phase change materials for thermal energy storage via direct impregnation method," *Journal of Thermal Analysis and Calorimetry*, vol. 123, no. 2, pp. 1173–1181, 2016.

[18] D. Mei, B. Zhang, R. Liu, Y. Zhang, and J. Liu, "Preparation of capric acid/halloysite nanotube composite as form-stable phase change material for thermal energy storage," *Solar Energy Materials and Solar Cells*, vol. 95, no. 10, pp. 2772–2777, 2011.

[19] L. Feng, J. Zheng, H. Yang, Y. Guo, W. Li, and X. Li, "Preparation and characterization of polyethylene glycol/active carbon composites as shape-stabilized phase change materials," *Solar Energy Materials and Solar Cells*, vol. 95, no. 2, pp. 644–650, 2011.

[20] Y. Wang, T. D. Xia, H. Zheng, and H. X. Feng, "Stearic acid/silica fume composite as form-stable phase change material for thermal energy storage," *Energy and Buildings*, vol. 43, no. 9, pp. 2365–2370, 2011.

[21] Z. Zhang, N. Zhang, J. Peng, X. Fang, X. Gao, and Y. Fang, "Preparation and thermal energy storage properties of paraffin/expanded graphite composite phase change material," *Applied Energy*, vol. 91, no. 1, pp. 426–431, 2012.

[22] J. Yang, G. Qi, Y. Liu et al., "Hybrid graphene aerogels/phase change material composites: thermal conductivity, shape-stabilization and light-to-thermal energy storage," *Carbon*, vol. 100, pp. 693–702, 2016.

[23] K. Yuan, Y. Zhou, W. Sun, X. Fang, and Z. Zhang, "A polymer-coated calcium chloride hexahydrate/expanded graphite composite phase change material with enhanced thermal reliability and good applicability," *Composites Science and Technology*, vol. 156, pp. 78–86, 2018.

[24] D. H. Atha and K. C. Ingham, "Mechanism of precipitation of proteins by polyethylene glycols. Analysis in terms of excluded volume," *Journal of Biological Chemistry*, vol. 256, no. 23, pp. 12108–12117, 1981.